Microwave radiometry experiment for snow in Altay China: time series of *in situ* data for electromagnetic and physical features of snow pack

Liyun Dai[1], Tao Che[1,2]*, Yang Zhang[1], Zhiguo Ren[1, 3], Junlei Tan[1], Meerzhan Akynbekkyzy[1], Lin Xiao[1], Shengnan Zhou[1], Yuna Yan[3], Yan Liu[4], Hongyi Li[1], Lifu Wang[5]

[1]Key Laboratory of Remote Sensing of Gansu Province, Heihe Remote Sensing Experimental Research Station, Northwest Institute of Eco-Environment and Resources, Chinese Academy of Sciences, Lanzhou, 730000, China.

[2]Center for Excellence in Tibetan Plateau Earth Sciences, Chinese Academy of Sciences, Beijing, 100101, China.

[3]University of Chinese Academy of Sciences, Beijing, 1000101, China.

[4] Institute of Desert Meteorology, China Meteorological Administration, Urumqi, 830002, China

[5]Altay National Reference Meteorological station, China Meteorological Administration, Altay, 836500, China.

Correspondence to: Tao Che (chetao@lzb.ac.cn)

Abstract. In this paper, we present a comprehensive experiment, namely, Integrated Microwave Radiometry Campaign for snow (IMCS), in Xinjiang, China, during snow season of 2015/2016. The campaign hosted a dual polarized microwave radiometer operating at L, K and Ka bands to provide minutely passive microwave observations of snow cover at a fixed site, along with daily manual snow pit observation of snow physical parameters, automatic observation of ten-minute 4-component radiation and layered snow temperatures, and meteorological observation of hourly weather data and soil data. To the best of our knowledge, our dataset is unique in providing continuous daily snow pits data and coincident microwave brightness temperatures, radiation and meteorological data, at a fixed site over a full season, which can be straightforwardly used for evaluation and development of microwave radiative transfer models and snow process models, along for land surface process and hydrology models. The consolidated data are available at http://data.tpdc.ac.cn/zh-hans/data/df1b5edb-daf7-421f-b326-cdb278547eb5/ (doi: 10.11888/Snow.tpdc.270886) (Dai, 2020).

Key words: Snow, Microwave radiometry, Snow pit, Experiment

1 Introduction

Field experiments/campaigns, as the main and most important approach for snow studies, have been conducted to obtain the electromagnetic and physical characteristics of snow cover. The main experiments/campaigns are summarized in table 1. The Cold Land Processes Field Experiment (CLPX) (https://nsidc.org/data/clpx/index.html), one of the most well-known experiments, was carried out from winter of 2002 to spring of 2003 in Colorado, USA (Cline et al., 2003). During the campaign, snow pits

were collected to coincide with airborne and ground remote sensing observations. In 2017, NASA SnowEx campaign (https://nsidc.org/data/snowex) was conducted in Colorado to test and develop algorithms for measurement of SWE in forested and non-forested areas by providing multi-sensor observations of seasonally snow-covered landscapes (Brucker et al., 2017). The campaign is still ongoing and will be conducted in other areas with different snow conditions. In northern Canada, mobile sled-mounted microwave radiometers were deployed in forest, open and lake environments from November 2009 to April 2010 and snow characteristics within the footprints of radiometers were measured to improve the understanding of the influence of snow characteristics on brightness temperatures (Derksen et al., 2012; Roy et al., 2013). The aforementioned microwave experiments were conducted at different sites for different land cover, resulting in good representativity for evaluating snow microwave emission model (Tedesco and Kim, 2006; Royer et al., 2017), however, with relative short temporal range, while dense temporal resolution is important to reveal the evolution of snow characteristics.

In the Arctic region, the Nordic Snow Radar Experiment (NoSREx) campaign was conducted at a fixed field of the Arctic boreal forest area in Sodankylä, Finland, during 2009 ~ 2013 (Lemmetyinen et al., 2016). The experiment provided a continuous time series of active and passive microwave observations of snow cover spanning an entire winter season, with synchronous observations of snow pit weekly. In Asia, an experiment of radiation budget over snow cover (JERBES) was conducted in Japan. In the experiment, snow pit work at 3 or 4 day intervals was conducted simultaneously with radiation budget observations during winter of 1999/2000 and 2000/2001 to analyze the effects of snow physical parameters on albedo (Aoki et al., 2003). The NoSREx and JERBES experiments, for fixed field observation, provided improved time series of data than CLPX and SnowEx. Weekly observation could reflect general evolution process of snow characteristics but might miss some key details that occur at sub-weekly scales. In the Tibetan plateau with shallow snow cover, multiple years of microwave radiometry observation at L band were conducted to study passive microwave remote sensing of frozen soil (Zheng et al., 2019 and 2021; Zhang et al., 2021). However, in the long-term series of experiment, no snow pit was measured and the microwave radiometry observation was only performed at L band which is insensitive to snowpack.

Table 1. Summary of existing experiments for microwave and optical radiation and physical features of snowpack

Campaign	Location	Temporal range	Observation content
CLPX	Different sites in Colorado,	February and March of 2002 and 2003	Inconsecutive multiple sensor observation, including microwave radiometry over snow, and synchronous snow pit measurements at different sites with short temporal range
SnowEx-year 1	Grand Mesa, and Senator Beck Basin, Colorado	February of 2017	Inconsecutive multiple sensor observation, including microwave radiometry over snow, and synchronous snow pit measurements at different sites with short temporal range
CMRES[1]	Mobile observation at Forest, open and lake	November of 2009-April of 2010	Mobile microwave radiometry and snow pit observation within footprint of radiometer. Short temporal range and inconsecutive observation

	in the northern Canadian region		
NoSREx	Fixed site in Sodankylä, Finland	Snow season during 2009-2013	Consecutive microwave radiometry and SAR observation over snow, and weekly snow pit measurement
JERBS	Fixed site in Japan	Snow season during 1999-2000	Consecutive optical radiation observation over snow and consecutive snow pit measurement at 3 or 4-day interval
IMCS (Presented in this work)	Fixed site in China	November of 2015-March of 2016	Consecutive microwave radiometry and optical radiation observation, and consecutive daily snow pit measurements

Note: [1]CMRES: Microwave radiometry experiment on snow cover conducted in northern Canada

To understand the evolution of snow characteristics and their influence on passive microwave brightness temperatures and radiation budget, an integrated field experiment on snowpack was conducted during a full snow season, in Altay, China. The experiment was designed to cover periods from snow-free conditions to eventual snow melt-off during 2015/2016. The microwave radiometry measurements at L, K and Ka bands for multiple angles were complemented by a dual-polarized microwave radiometer with 4-component radiation and daily in situ observations of snow, soil and atmospheric properties, using both manual and automated methods. To the best of our knowledge, our dataset is unique in providing continuous daily snow pit observations over a full snow season at a fixed site, along with synchronous microwave brightness temperatures, radiation and meteorological data. The dataset is consolidated and organized, which can be easily used for other researchers with interests.

In the next section, the experiment location, parameters, and parameter measurement protocols are described. Section 3 introduces the consolidated data that was released at the National Tibetan Plateau Data Center, China, which provides data support for international science programs (Li et al., 2021; Pan et al., 2021). Section 4 presents content of brightness temperature, 4-component radiation, snow pit data, soil temperature and moisture, and meteorological data. Section 5 discusses the possible applications and uncertainties. Finally, the conclusions are summarized in section 6.

2 Description of experiment setup

2.1 Measurement location

The Integrated Microwave Radiometry Campaign for snow (IMCS) was performed during the 2015/2016 snow season (from November 27, 2015 to March 25, 2016) at the Altay National Reference Meteorological station (ANRMS) (N47°44'26.58", E 88°4'21.55"), which is approximately 6 km from the foot of Altay mountain in the northwest China (Figure 1). Altay mountain with elevation up to 3000 m, running northwest and southeast, is at the junction of China, Russia, Mongolia and Kazakhstan, providing snow water resources for these four countries. The average annual maximum snow depth measured in this station is approximately 40 cm, with a maximum over 70 cm. In the southwest of Altay mountain, crop land and desert with flat terrain are the dominant land covers. Snow cover is critical fresh

water for the irrigation in this area. In this experiment, measurements included microwave radiometry, 4-component radiation, snow pit and soil parameters. The test sites of this experiment were four neighboring bare rectangle fields in the ANRMS with areas of 2000 m^2 (Filed1 (F1) in Figure 1), 3000 m^2 (Field 2 (F2) in Figure 1), 400 m^2 (Field3 (F3) in Figure 1) and 300 m^2 (Field4 (F4) in Figure 1), respectively.

In the F2, the ground-based microwave radiometer was set up in the middle of the field, facing south to collect brightness temperatures over snow cover. F1 behind the microwave radiometers (north of the radiometers) was for manual snow pit data collection. The microwave radiometer observations and snow pit data collections were conducted by Northwest Institute of Eco-Environment and Resources, Chinese Academy of Science (NIEER) from November 27, 2015 to March 25, 2016 (snow free after March 25, 2016).

F3 was for meteorological measurements including wind speed, wind direction, air temperature, air wetness, air pressure, precipitation, soil temperature, soil moisture among others. These parameters were automatically obtained from instruments, and the instruments setup and data collection were operated by ANRMS. In this experiment, we requested the wind, air pressure, air wetness, air pressure, soil temperature and moisture data during this experiment from ANRMS. F4 was designed for automatic measurement of layered snow temperatures, snow density, SWE, snow depth, and albedo, with instruments operated by NIEER since 2013. However, during the experiment, the instruments for snow density and SWE were not functional, and we only collected layered snow temperatures and 4-component radiation.

Because the four observation fields, located within the domain of the station, are with distance less than 100 m, it is reasonable to assume that the snow characteristics and soil and weather conditions are consistent among these four fields.
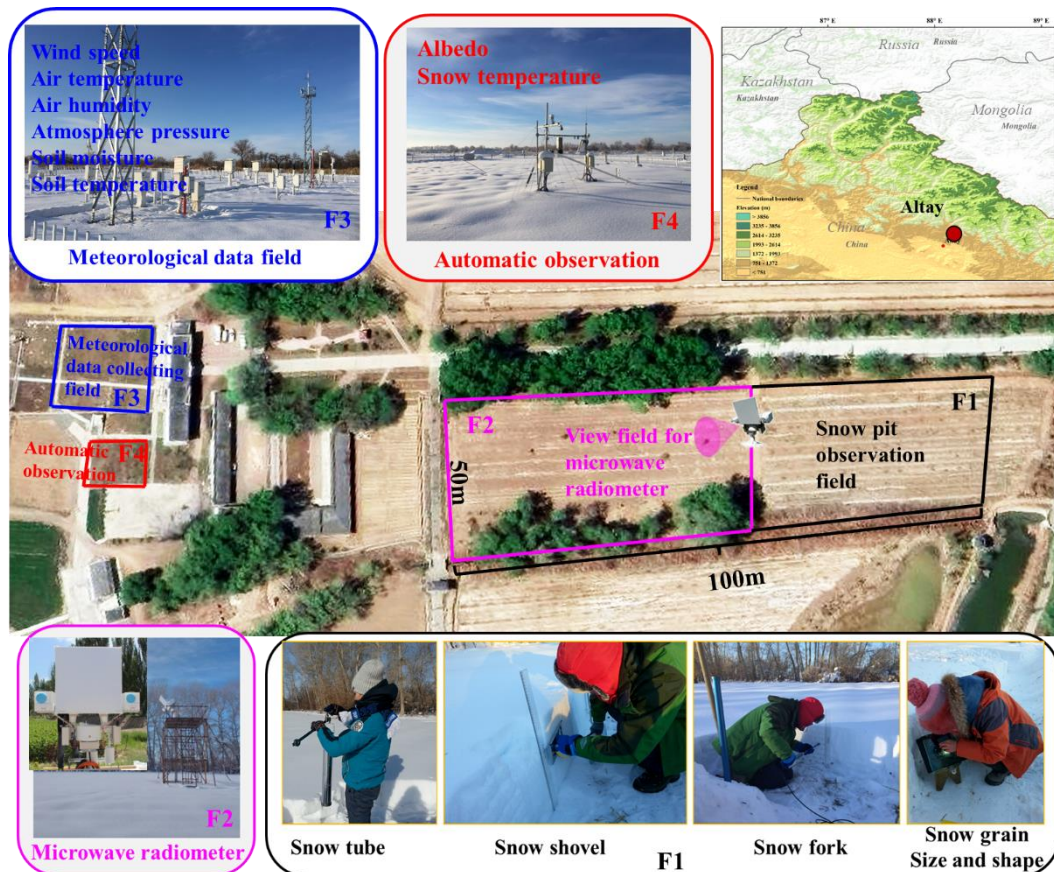
Figure 1. Location of the Altay National Reference Meteorological station (ANRMS) in Asia, along with the four test sites in the ANRMS. F1 (approximately 40 m × 50 m) was for snow layering, layer thickness, snow density, snow grain size and shape of each layer. F2 (approximately 60 m × 50 m) was for microwave radiometers observations. F3 was for meteorological and soil data collection operated by the ANRMS. F4 was for the automatically observation of the snow temperature, and 4-component radiation, designed by Northwest Institute of Eco-Environment and Resources, Chinese Academy of Science (NIEER).

2.2 Measurement methods

The microwave signatures from snowpack vary with snow characteristics, soil and weather conditions. In this experiment, the measurements include microwave radiometry observation to collect brightness temperature, manual snow pit observation to collect snow physical parameters, automatic observation to collect 4-component radiation and snow temperatures, and meteorological observation containing weather data and soil data.

2.2.1. Microwave radiometry

The brightness temperatures at 1.4 GHz, 18.6 GHz, and 36.5 GHz for both polarization (Tb1h, Tb1v, Tb18h, Tb18v, Tb36h, Tb36v) were automatically collected using a six-channel dual polarized microwave radiometer RPG-6CH-DP (Radiometer Physics GmbH, Germany, https://www.radiometerphysics.de/products/microwave-remote-sensing-instruments/radiometers/). The technical specifications of the RPG-6CH-DP are described in Table 2. The RPG-6CH-DP contains a built-in temperature sensor used for measuring air temperature. The automated data collection frequency was set to 1 minute.

141

142 **Table 2. Technical Specifications of the RPG-6CH -DP Microwave Radiometer.**

Parameter	Value
Manufacturer	Radiometer Physics GmbH
System noise temperatures	<900 K
Bandwidth	400MHz (20MHz for 1.4 GHz)
System stability	0.5 K
Dynamic range	0~400 K
Frequencies (GHz)	1.4, 18.7, 36.5
Polarizations	V, H
Internal calibration	Internal Dicke switch and software control for automatic sky tilt calibration
Receiver and antenna thermal stabilization	< 0.015 K
Antenna sidelobe level	< -30 dBc
Optical resolution (HPBW)	6.1º (11º for 1.4 GHz)
Incidence angle	0~90º
Azimuth angle	360º

143

144 Before the snow season, a platform with height of 5 m, length of 4 m and width of 2 m was
145 constructed in the experiment field (Figure 2). A 4-m orbit was fixed on the platform. The RPG-6CH-DP
146 was set up on the orbit and could be moved along the orbit. The microwave radiometers at K and Ka
147 bands began working from November 27, 2015, while the L band radiometer began working since
148 January 30, 2016. These radiometers were sky tipping calibrated, with accuracy of 1 K. In clear sky
149 conditions, the sky brightness temperatures were approximately 29.7$\pm$0.3 K at 18.7 GHz and 29.3$\pm$0.9
150 K at 36.5 GHz for both polarizations. While the sky brightness temperatures at L band showed large
151 fluctuation. They ranged from -1 to 8 K for horizontal polarization, and 1 to 16 K for vertical polarization.

152 Generally, the radiometers were fixed in the middle of the orbit to observe snow cover with incidence
153 angle of 50º. Multi-angle observations were conducted after every big snowfall, or every 5 days in the
154 stable period. In the melt period, observation frequency increased. There are total seventeen multi-angle
155 observation on December 3, 19, and 30; January 3, 8, 13, 18, 3, and 28; February 3; March 3, 10, 15, 22,
156 26, 28, and 31, when the radiometer was set to scan the ground at different incidence angles at the left,
157 middle and right of the orbit, respectively. Although the view fields of the antennas for 1.4 GHz, 18.7
158 GHz and 36.5 GHz did not completely overlap, the measured results showed that the brightness
159 temperatures observed at the left, middle and right of the orbit varied within 1 K. Therefore, the snow
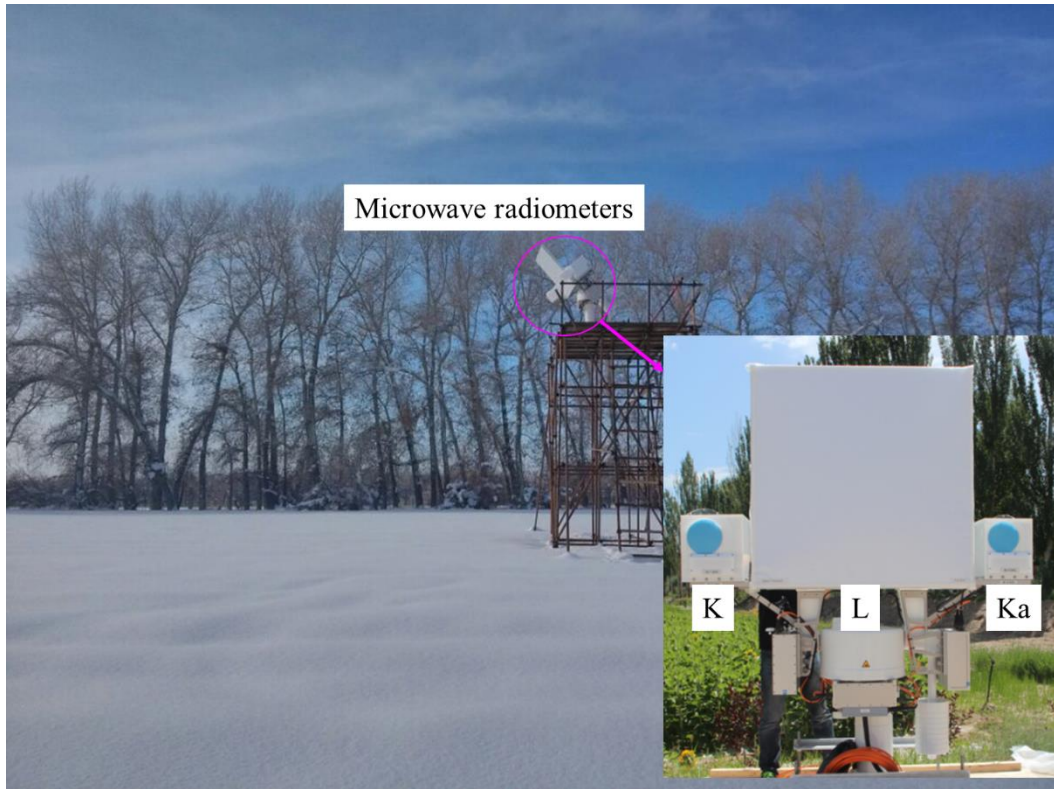160 and soil conditions were considered homogeneous within the view fields of the three antennas.

Figure 2. Ground-based microwave radiometer observation system.

2.2.2 Snow pit measurement

The snow characteristics, including snow layering, snow layer thickness, grain size, snow density, and snow temperature, were collected by manual snow pit measurements in the black field. These data were daily collected during 8:00-10:00 am local time, from November 27, 2015 to March 25, 2016, except 7 days (please see Table 3). Although the snow temperatures were manually measured at snow pits, the automatically collected snow temperatures in the red field were utilized in this study, because the temperature measured at snow pits could not reflect the natural temperature profile when the snow pits exposed to air.

Table 3. Variables collected by manual daily snow pit measurement in black field in figure 1, along with their observation instruments, observation time and frequencies.

Parameter	Instruments	Precision	Layering style	Observation time or frequency	Absent date
Layer thickness (cm)	Ruler	0.1cm	Natural layering	local time 8:00-10:00 am	no
Snow density (g/cm^3)	Snow tube (Chinese Meteorological Administration)	pressure:0. 1g/cm^2, snow depth: 0.1 cm	Whole snowpack		no
Snow density (g/cm^3)	Snow shovel (NIEER)	weight: 0.01g, volume: 1cm^3	Every 10 cm		January 2-3, 2016;

7

Snow density (g/cm^3) and	Snow fork (Toikka Enginnering Ltd.)	0.0001g/cm^3	Every 5 cm	February 20, 2016
Liquid water content (%)	Snow fork	0.001%	Every 5 cm	
Snow grain size (mm)	Anyty V500IR/UV	0.001mm	Natural layering	December 24, 31, 2015; January 1-3, 23, 2016, February 20, 2016
Snow grain shape	Shape card	N/A	Natural layering	

The first step of snow pit measurement is making a snow pit. In the black field, a new snow pit was dug each day using a spade. The snow pit was approximately 2 m x 1m to make sure all parameters could be measured from unbroken snowpack. The snow pit section was made as flat as possible using a flat shovel or ruler. When the snow profile is exposed to air for a long time, the snow characteristics will be influenced by environment and will be different from the natural snow characteristics. In order to make sure every observation conducted on natural snow pit, the snow pit was backfilled with the shoveled snow after finishing all observations, and the new snow pit in the following day was made at least 1-m distance away from the latest snow pit. After finishing a snow pit, the natural snowpack stratification was then visually determined, and the thickness of each layer was recorded against a ruler.

The next step was measuring grain size and shape type in each layer. The grain size and type within each natural layer were estimated visually using a microscope with an "Anyty V500IR/UV" camera (Figure 3a). The software "VIEWTER Plus" matched the microscope was used to measure grain size. The grain type was determined based on Fierz et al. (2009). In this experiment, we utilized the length of longest axes and the length of shortest axes to describe grain size (Figure 3b). When using the software to measure the grain size, a reference must be needed. In this experiment, a ruler marked 0.5 mm was used as a reference (Figure 3c). We adjusted the focus of the camera to make sure the grains at the clearest status in camera to take photos, and the photo of ruler scale was taken at the same focus. If the thickness of one layer was less than 10 cm, measurements were performed at the top and bottom of the layer, respectively. If the thickness was greater than 10 cm, measurements were performed at the top, middle, and bottom of the layer, respectively. For each layer, at least 5 photos were taken, and the longest axes length and the shortest axes length of at least 10 typical grains were recorded. The final grain size was the average of the 10-group recorded values. Figure A1 presents an example of the original photos of grains in each layer, and Table A1 shows the matched record of longest and shortest axis length.

      (a)   (b)   (c)

Figure 3. (a) Picture of microscope "Anyty V500IR/UV", (b) the measured longest axes lengths and shortest axes length of particles, and (c) the reference ruler scale.

Snow density was measured using three instruments: snow tube, snow shovel and snow fork (Figure 4). The snow tube instrument, designed by Chinese Meteorological administration, contains a metal tube with the base area of 100 cm^2 and the length of 60 cm, and a balance (figure 4a). It was utilized to measure the snow density of a whole snowpack by weighing the snow sample. The snow shovel is a 1500 cm^3 wedge-type sampler, and its length, width and height are 20 cm, 15 cm, and 10 cm, respectively (figure 4b). It was utilized to measure snow density every 10 cm (0-10 cm, 10-20 cm, 20-30 cm…). The snow fork (figure 4c) is a microwave resonator that measures the complex dielectric constant of snow, and adopts a semi-empirical equation to estimate snow density and liquid water content based on the complex dielectric. It was utilized to measure snow density and liquid water content at 5-cm intervals starting 5 cm above the snow/soil interface (5cm, 10cm, 15 cm, 20cm…). In order to decrease the observation error, every measurement repeated three times. If there was an abnormal value, a fourth measurement would be performed to ensure the accuracy. Table A2 is an example record table for snow density. The average value of the three-time observation was the final value.


      (a)   (b)   (c)
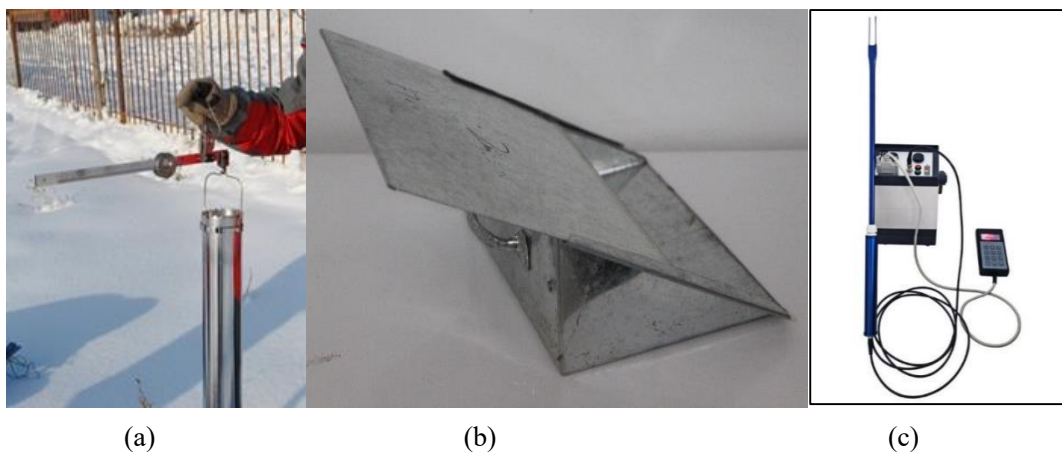
Figure 4. Three instruments for snow density: (a) Snow tube, (b) Snow shovel, and (c) Snow fork.

2.2.3 Automatic radiation and temperature measurement

In the red field, the 4-component radiation was automatically measured by Component Net Radiometer (NR01) manufactured by Hukseflux, and layered snow temperatures was measured by Campbell 109S temperature sensors, respectively. The temperature sensors were set up on a vertical pole inserted in soil (Figure 5). The sensors' heights are 0 cm, 5 cm, 10 cm, 15 cm, 25 cm, 35 cm, 45 cm, and 55 cm above soil/snow interface, and temperatures were collected every ten minute.

The NR01 net radiometer was set up to measure the energy balance between incoming short-wave and long-wave far infrared radiation versus surface-reflected short-wave and outgoing long-wave radiation. The range of short wave is 285~3000nm, and the range of long wave is 4.5~40 um. The 4-component radiation was automatically recorded every ten minutes. In addition, the sensor was equipped with a Pt100 temperature sensor for parallel recording of the sensor temperature.
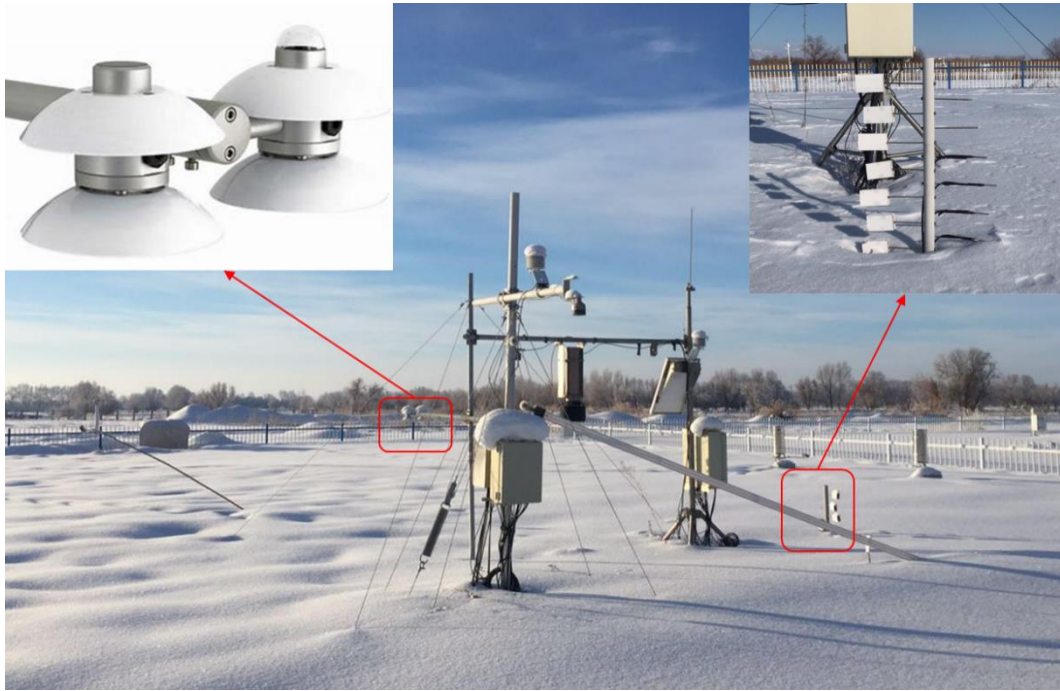
234

235 **Figure 5. Set up of temperature sensors and CNR01 in the red field.**

236

237 **2.2.4 Meteorological observation**

238   The meteorological data include air temperature, air pressure and humidity, wind speed, soil

239 temperature at -5 cm, -10 cm, -15 cm and -20 cm, and soil moisture at -10 cm and -20 cm. These

240 parameters are routine observations conducted at ANRMS. The instruments used for soil and weather

241 parameters observations are produced by China Huayun Meteorological Technology Group Corporation.

242 The measurement parameters and their measurement instruments are listed in table 4.

243 **Table 4. Automatically observed variables and the observation instruments, observation time and**

244 **frequencies.**

Parameter	Instruments	Precision	Layering style	Observation time or frequency
Snow temperature(°C)	Temperature sensors (Campbell 109S)	0.001 °C	0 cm, 5 cm, 10 cm, 15 cm, 25 cm, 35 cm, 45 cm, and 55 cm	Ten-minute
4-component radiation (W/m²)	Component Net Radiometer NR01 (Hukseflux)	0.001 W/m²	6 feets above ground	Ten-minute
Soil temperature (°C)	Soil temperature sensor (China Huayun)	0.1 °C	-5cm, -10 cm, -15cm and -20 cm	Hourly
Soil moisture (%)	Soil moisture sensor (DZN3, China Huayun)	0.1%	-10 cm and -20 cm	Hourly
Air temperature (°C)	Thermometer screen (China Huayun)	0.1 °C	6 feet above ground	Hourly

Air pressure (hPa)	Thermometer screen (China Huayun)	0.1 hPa	6 feet above ground	Hourly
Air humidity (%)	Thermometer screen(China Huayun)	1%	6 feet above ground	Hourly
Wind speed (m/s)	Wind sensor(China Huayun)	0.1m/s	10 m above ground	Hourly

The air temperature, pressure and humidity were collected using temperature and wetness sensor in thermometer screen. The wind speed and direction were measured using wind sensor set up at 10 m on a tower. Soil moisture and temperature were automatically measured using moisture sensor and temperature sensor. Figure 6 depicts the instruments for these observations.

<div align="center">(a)   (b)   (c)   (d)</div>

Figure 6. Instruments for observation of (a) air temperature and wetness, (b)wind speed, (c) soil temperature and (d) soil moisture.

3 Description of consolidated IMCS dataset

The microwave brightness temperature, snow parameters, meteorological data were recorded in different formats, and their observation frequencies and times were different. These data must be reorganized and consolidated for ease of use. The values from the three-time measurements for snow density in each layer were averaged to obtain the final snow density. The length of the longest and shortest axes of particles in each photo were measured using the software. The average lengths of longest and shortest axes from all photos in each layer were obtained as the final grain size. The daily snow pit data were finally consolidated into a NetCDF file "snow pit data.nc".

The time series of automated layered snow temperature and 4-component radiation data were first processed by removal of abnormal values and gap fill, and then consolidated into a NetCDF file "ten-minute 4 component radiation and snow temperature.nc". The ground-based brightness temperatures and the formatted weather and soil data requested from ANRMS were provided 'as is'. Brightness temperature data were divided into time series of brightness temperature and multi-angle brightness temperatures, and separately stored in two NetCDF files. The weather and soil data were consolidated into a NetCDF file "hourly meteorological and soil data.nc". Table 3 describes the contents of the provided dataset.

1) Brightness temperatures data:

271   Minutely brightness temperature at 1.4 GHz, 18 GHz and 36 GHz for both polarizations at incidence

272   angle of 50°. This data include time, incidence angle, azimuth angle, and brightness temperatures at the

273   three bands for both polarizations.

274   Seventeen groups of calibrated brightness temperature at 1.4 GHz, 18.7 GHz and 36.5 GHz for both

275   polarizations at different incidence angles (30, 35, 40, 45, 50, 55, 60°). This data include time, incidence

276   angles, azimuth angle, and brightness temperatures at the three bands for both polarizations.

277   **2) Manual snow pit data:**

278   Daily snow pit data include date, snow depth, layered snow thickness, average longest axis, average

279   shortest axis, grain shapes of each layer; layered snow density using snow fork (snow density at different

280   heights, such as SF_5cm, SF_10cm, SF_15cm), snow density using snow tube, layered snow density

281   using snow shovel (such as SS_0-10cm, SS _10-20cm, SS _20-30cm, SS _30-40cm).

282   **3) Automated snow temperature and radiation data**

283   Ten-minute 4-component radiation and snow temperature data include time, short-wave incident

284   radiation, short-wave reflected radiation, long-wave infrared incident radiation, long-wave infrared

285   reflected radiation, sensor temperature, and snow temperatures at different heights (such as ST_0cm,

286   ST_5cm)

287   **4) Meteorological and soil data:**

288   Hourly weather data include time, air temperature, pressure, humidity, wind speed, soil temperature

289   at 5 cm, 10 cm, 15 cm and 20 cm, and soil moisture at 10 cm and 20 cm.

290

291   **Table 3. Description of consolidated data**

Data	Content	File name	Variables
Brightness temperature	Brightness temperature	TBdata.nc	Time (yyyy-mm-dd hh:mm:ss), Tb1h, Tb1v, Tb18h, Tb18v, Tb36h, Tb36v, incidence angle, azimuth angle
	Multi-angle brightness temperatures	TBdata-multiangle.nc	Time (yyyy-mm-dd hh:mm:ss) , Tb1h, Tb1v, Tb18h, Tb18v, Tb36h, Tb36v, incidence angle, azimuth angle
Manual snow pit data	Layer thickness, layered grain size and shape, snow density	Daily snow pit data.nc	Time (yyyy-mm-dd), snow depth, th1, Lg1, Sg1, th2, Lg2, Sg2,th3, Lg3, Sg3, th4, Lg4, Sg4, th5, Lg5, Sg5, th6, Lg6, Sg6, Stube, SS_0-10, SS_10-20, SS_20-30, SS_30-40, SS_40-50, SF_5, SF_10, SF_15, SF_20, SF_25, SF_30, SF_35, SF_40, SF_45, SF_50, shape1, shape2, shape3, shape4, shape5, shape5
Automated snow temperature and radiation data	4-component radiation, snow temperature	Ten-minute 4 component radiation and snow temperature.nc	Time (yyyy-mm-dd hh:mm), SR_DOWN, SR_UP, LR_DOWN, LR_UP, T_Sensor, ST_0cm, ST_5cm, ST_15cm, ST_25cm, ST_35cm, ST_45cm, ST_55cm
Meteorological and soil data	meteorological data, soil moisture and temperature	Hourly meteorological and soil data.nc	Time (yyyy-mm-dd hh), Tair, Wair, Pair, Win, SM_10cm, SM_20cm, Tsoil_5cm, Tsoil_10cm, Tsoil_15 cm, Tsoil_20cm

292   Note: th: snow thickness, Lg: long axis, Sg: short axis, shape: grain shape;

293   Stube: snow density observed using snow tube, SS: snow density observed using snow shovel, SF: snow density

294   observed using snow fork; ST: snow temperature; SR_DOWN: downward short-wave radiation, SR_UP: upward

short-wave radiation, LR_DOWN, downward long-wave radiation, LR_UP: upward long-wave radiation, T_sensor:

sensor temperature; Tair: air temperature, Wair: air wetness, Pair: air pressure, Win: wind speed.

4 Overview and preliminary analysis of collected data from IMCS

4.1 Snow characteristics

4.1.1 Layering grain size and grain shape

During 2015/2016, snow cover began on November 25, 2015, and ended on March 25, 2016. During this snow season, there were seven snowfall events and each formed a distinct snow layer except for the third event whose layering was indistinguishable from the second layer (Figure 7 gray). The fourth event was the biggest. After, the snow depth started to decrease and the snow density increased. Snow cover began melting on March 14 and ended within 10 days.

Grain sizes within all layers increased during the snow season, except in the bottom layer where grain size experienced a decrease from December 28 to January 20 (Figure 8). In the vertical profile, grain size increased from top to bottom with the snow age. The grain size of the fresh snow was approximately 0.3 mm during the experiment. The biggest long and short axis, occurring in Layer 1 during the melt period, were up to 6 cm and 4 cm, respectively. The length of short axes is approximately 0.7 of the length of long axes. The grain shape generally developed from rounded grains to facet crystals, and then to depth hoar. After March 13, 2016, the minimum air temperature increased to above 0°C, snowmelt accelerated, and the grain shape developed to melted forms (Figure 7).
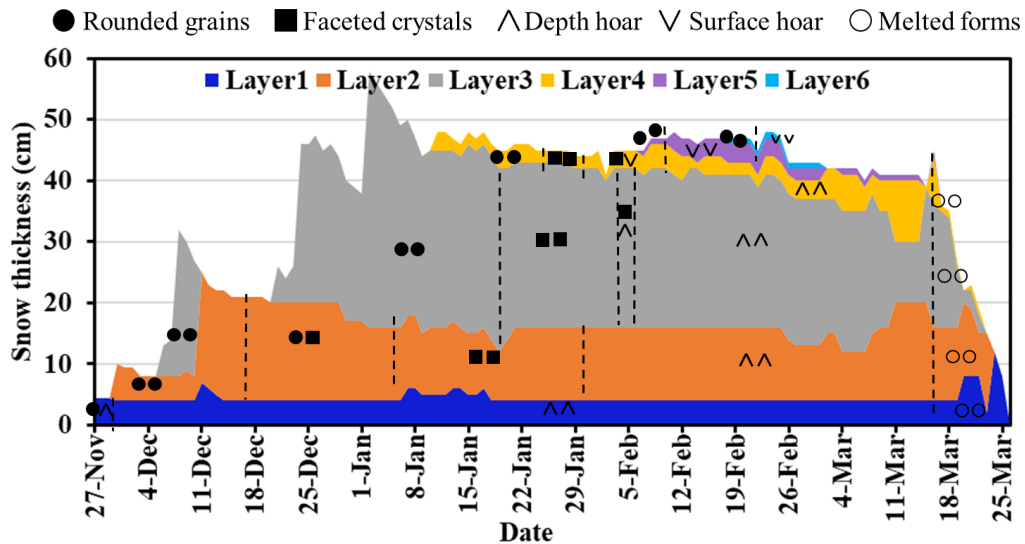
**Figure 7. Daily variation in snow layers and grain shape in each layer from November 27, 2015 to March 25, 2016.**
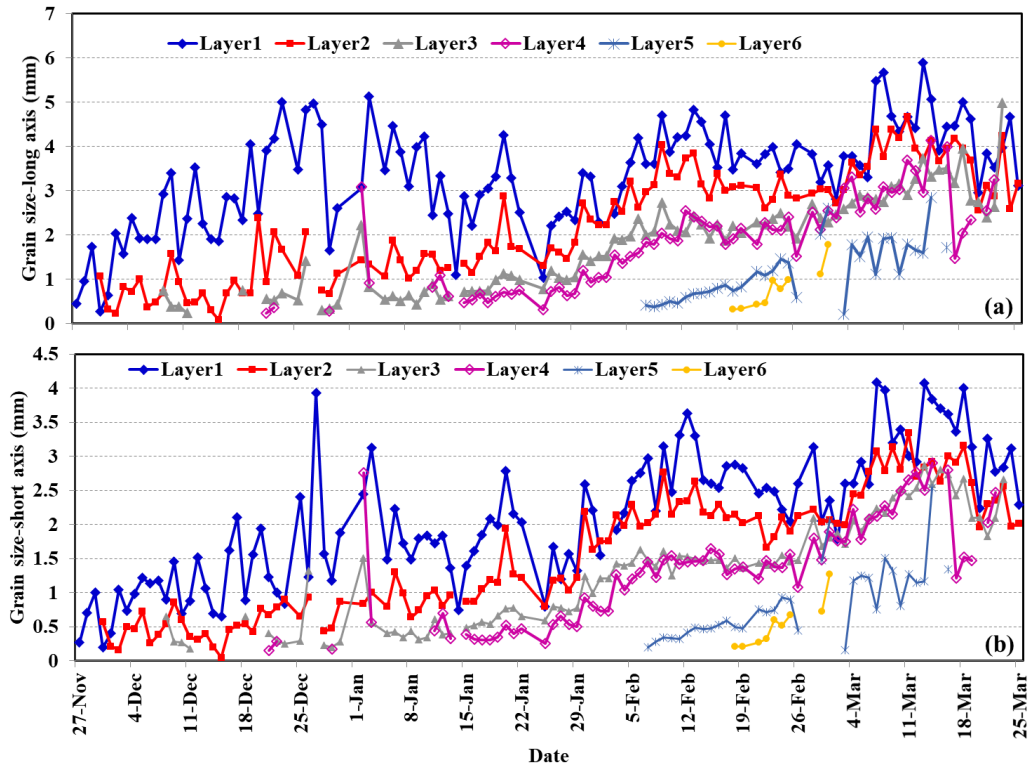
Figure 8. Daily variation in grain size within each layer from November 27, 2015 to March 25, 2016. The layer thicknesses are presented in figure 7.
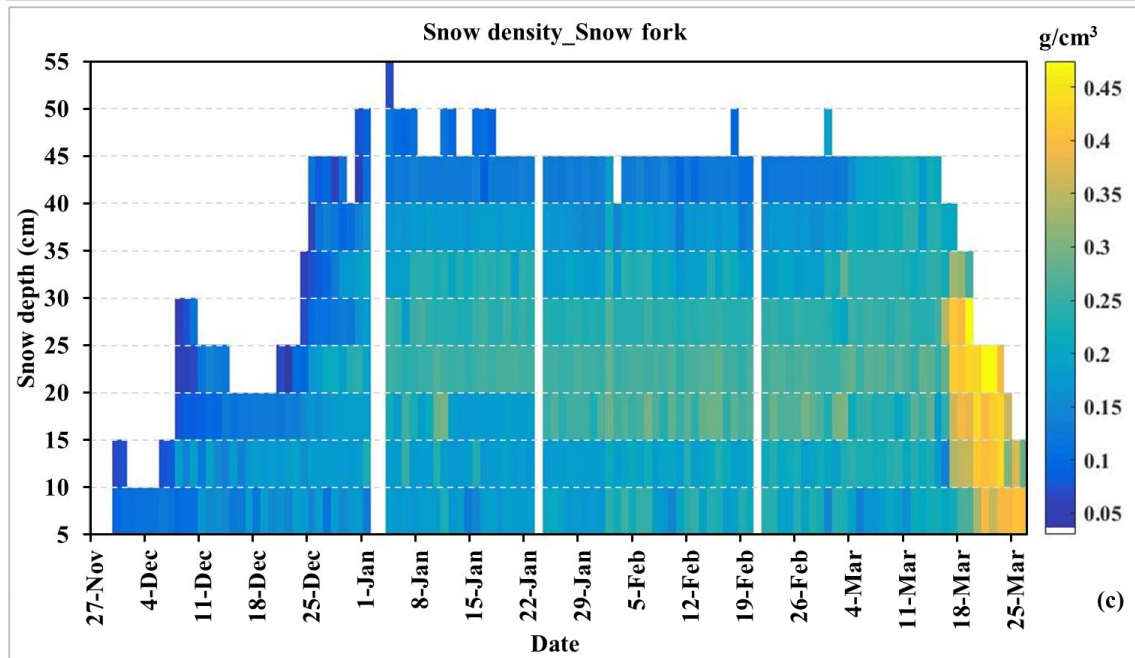
4.1.2 Snow density

Snow density measured by three different instruments shows that the density of fresh snow ranged between 0.05~1.0 g/cm^3 (Figure 9). The snow densities increased with snow age, and remained stable after reaching ~0.2-0.25 g/cm^3. From March 14 on, snow densities abruptly increased, with the maximum value over 0.45 g/cm^3. In the vertical profile, snow density increased from top to bottom in the accumulation phase. However, after January 3, 2016, snow densities in the middle layers were larger than those in the bottom and upper layers due to the well-developed depth hoar of bottom layer. In the melting phase, there were no significant diffferent for the snow densities in all layers. Snow fork provided most detail snow density profile, but systematically underestimated snow density compared with snow tube and snow shovel by 24% (Dai et al., 2022).

333

(b)

334

Snow density_Snow fork

(c)
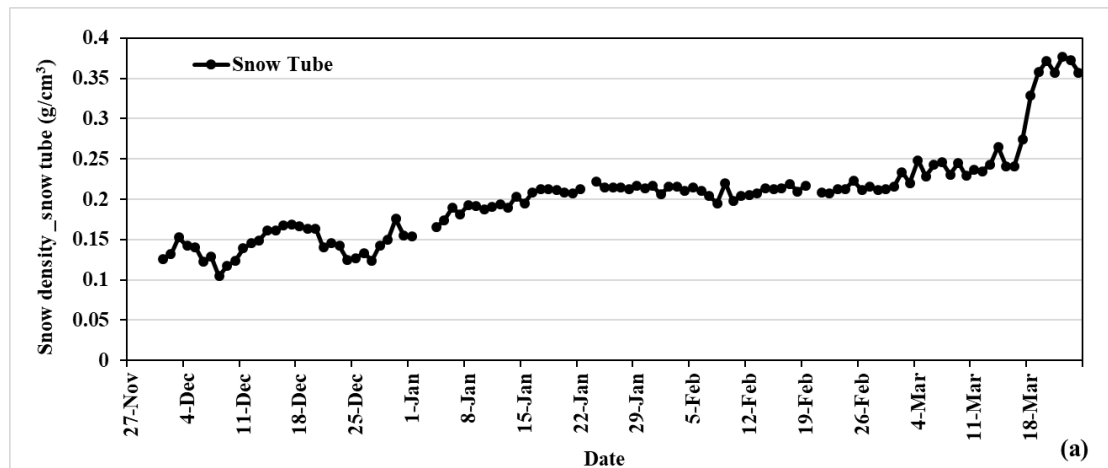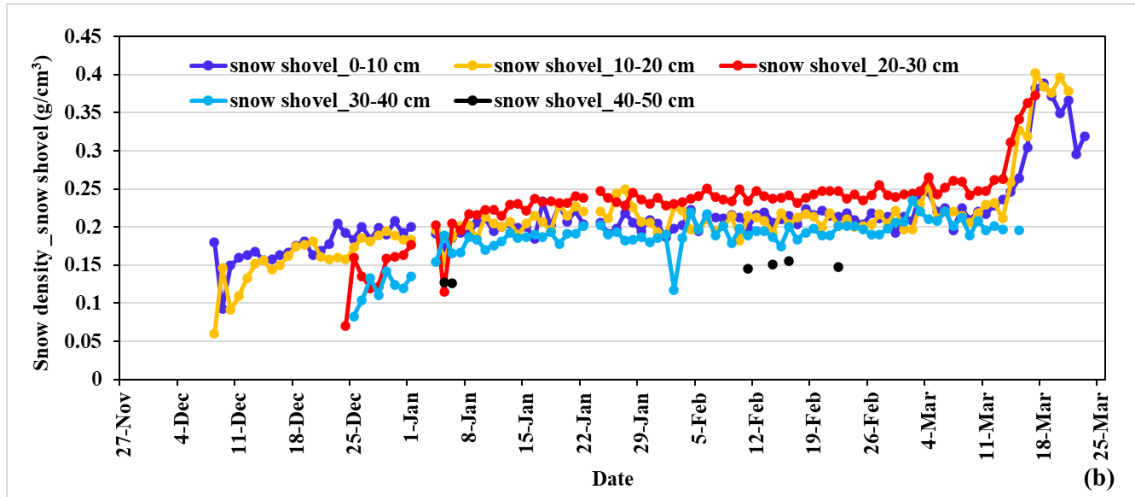
335 **Figure 9. Daily variation in snow densities measured using three different measurement methods from**
336 **November 27, 2015 to March 25, 2016, (a) overall snow density measured using snow tube, (b) snow density**
337 **at 10-cm interval using snow shovel, and (c) snow density at 5-cm interval using snow fork.**

338

339 **4.1.3 Snow temperature**

340   The diurnal range of snow temperature decreased from top to bottom layers. As the snow depth
341 increased, there were more layers with small diurnal variations (Figure 10). Snow temperature at 0 cm
342 (snow/soil interface temperature) showed no significant diurnal variation, remaining at approximately -
343 2.0 to 0.7 °C. Snow temperature in the top layer had the largest diurnal variation. After March 17, 2016,
344 the snow temperature of all layers were over 0°C, implying that snow cover did not refreeze anymore.

345
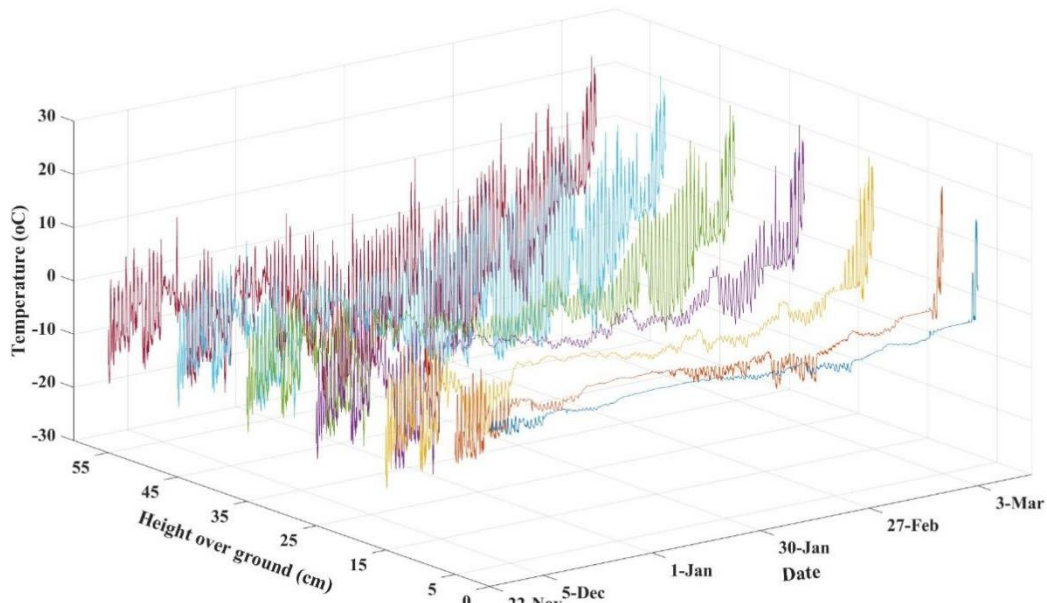
Figure 10. Minutely variation in snow temperatures at 0 cm (snow/soil interface), 5 cm, 15 cm, 25 cm, 35 cm, 45 cm and 55 cm above ground during experiment period

4.2 Soil temperature and moisture

The soil temperature at 5 and 10 cm remained stable and below 0 °C during the snow season but presented large fluctuation before (after) snow on (off) (Figure 11). The temperature difference between 5 cm and 10 cm was much larger before snow cover onset than during snow cover period. The soil moisture at 10 cm were above 10% before snow cover onset and after snow off. There were two soil moisture peaks within the snow cover period, one from December 12-14 and the other from January 1-20.

355
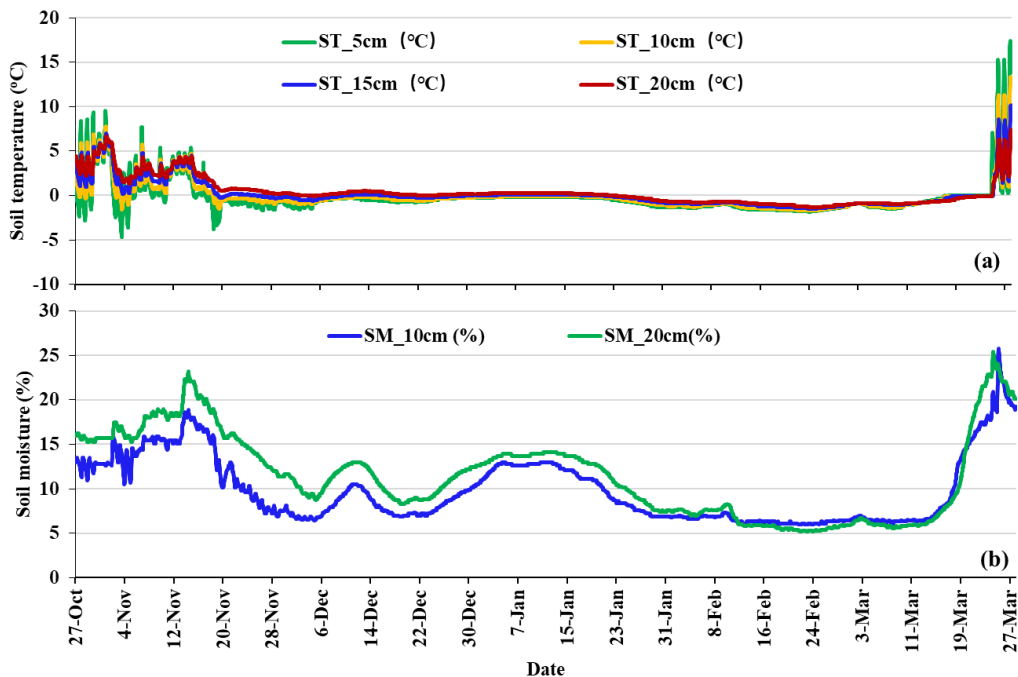
Figure 11. (a) Hourly soil temperature at 5 cm, 10 cm, 15 cm and 20 cm below the snow/soil interface (a), and (b) soil moisture at 10 cm and 20 cm below the snow/soil interface.
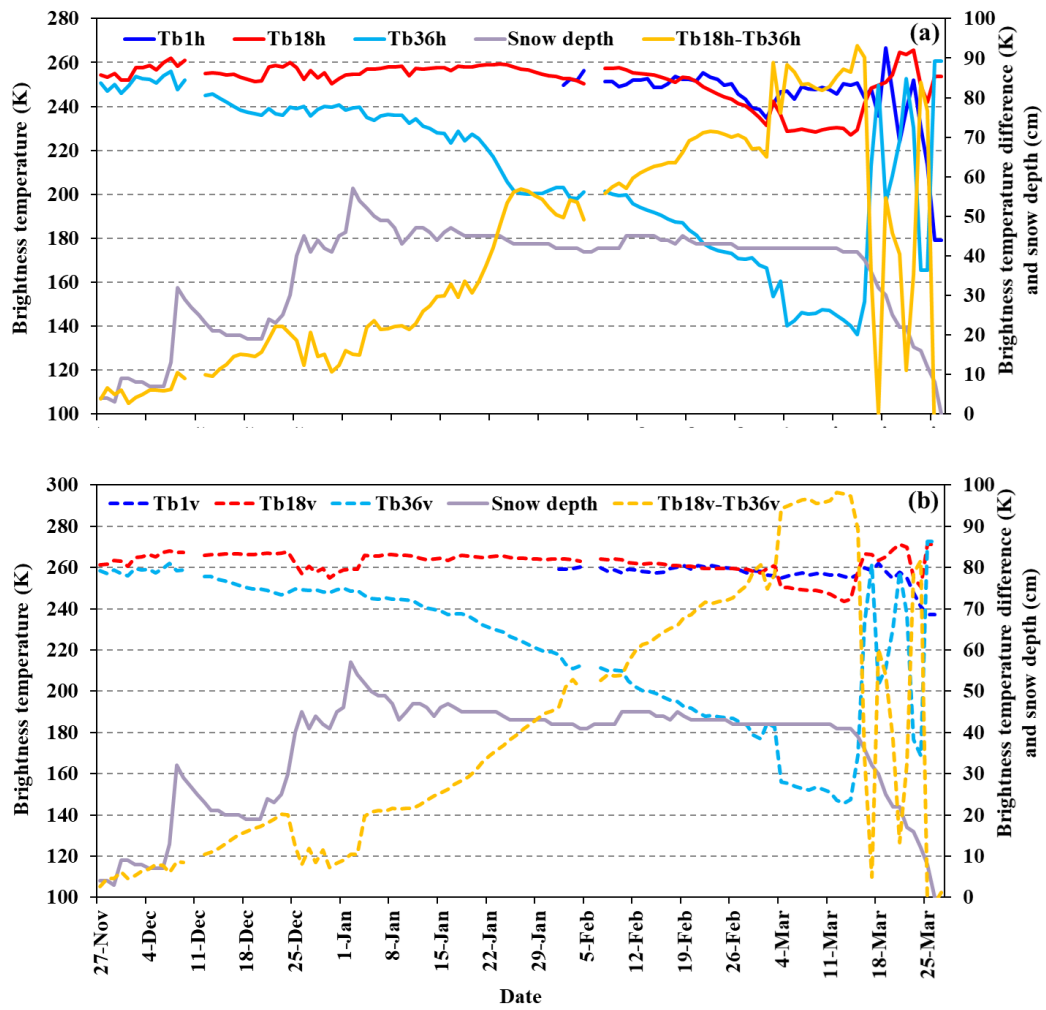
4.3 Brightness temperature

The microwave brightness temperatures varied with snow, soil, and weather conditions. Figure 12 shows the daily brightness temperatures, brightness temperature difference between 18 and 36 GHz, and snow depth at 1:00 am local time. Figure 13 shows the hourly variation in brightness temperatures at 1.4 GHz, 18.7 GHz and 36.5 GHz and air temperature after February 1. Data show that Tb36h and Tb36v decreased during the full snow season, Tb18h exhibited an obvious decline after February 18, and Tb18v after March 3 (Figure 12). After January 4, though snow depth stopped increasing, the brightness temperature continued to decrease and brightness temperature difference increased. Based on Figure 8, snow density became stable after January 15. Therefore, after January 4, the decreasing brightness temperatures was mainly caused by growing grain size. The variation of L band mainly relies on soil moisture and soil temperature change. We have soil temperatures at 0 cm, 5 cm and 10 cm and soil moisture at 10 cm. However, the L band reflects the soil moisture within 5 cm which was absent in this experiment.

After February 25, brightness temperature exhibited a distinct cycle of daytime increase and nighttime decrease (Figure 13), resulting from large liquid water content caused by high daytime air temperature (above 0 °C) and the melted snowpack refreezing at nighttime. After March 14, there was another big rise in air temperature and even the nighttime air temperatures were above 0°C. During this period of accelerated snowmelt, as the liquid water within the snowpack did not refreeze completely at night, both brightness temperatures at three bands and brightness temperature difference exhibited irregular behavior.

380

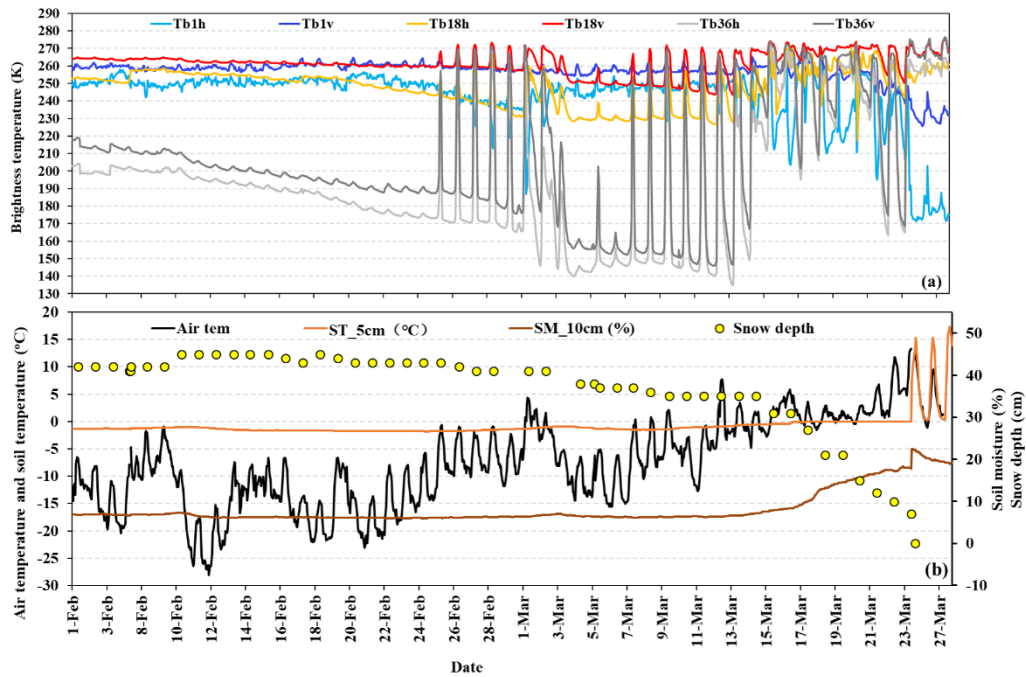**Figure 12. Daily variations in brightness temperatures at 1.4 GHz, 18 GHz and 36 GHz, for horizontal**

(Tb1h, Tb18h, Tb36h) and vertical polarizations (Tb1v, Tb18v, Tb36v), the differences between Tb18h and

Tb36h (Tb18h - Tb36h), and between Tb18v and Tb36v (Tb18v - Tb36v), at 1:00 am local time, from

November 27, 2015 to March 26, 2016. (a) for horizontal polarization, and (b) for vertical polarization.

385

386

387

18

Figure 13. Hourly variation in (a)Tb1h, Tb18h, Tb36h, Tb1v, Tb18v, and Tb36v, and (b) air temperature, soil moisture at 10 cm and soil temperature at 5 cm, and daily variation in snow depth, from February 1 to March 28, 2016.

The brightness temperatures at 18.7 and 36.5 GHz from AMSR-2 and at 1.4 GHz from SMAP were compared with the ground-based observations at the overpass time (Figure 14). Although there were large differences between satellite and ground-based observations, the general temporal patterns were the same. Specifically, the abrupt changes at 18.7 and 36.5 GHz on March 3 and March 16 were captured by both satellites and ground-based sensors. Brightness temperatures at 1.4 GHz from both SMAP and ground microwave radiometer kept stable before March 16, after when, brightness temperature rapidly decreased because of the increase of soil moisture. The correlation coefficients at both polarizations were approximately 0.96, 0.7 and 0.88 for 36.5 GHz, 18.7 GHz and 1.4 GHz, respectively. Satellite observed brightness temperature presented less decrease trend than ground-based observation. The difference at 36.5 GHz is larger than those at 18.7 and 1.4 GHz. The difference between ground-based and satellite observation might be attributed to the different field of views.

19
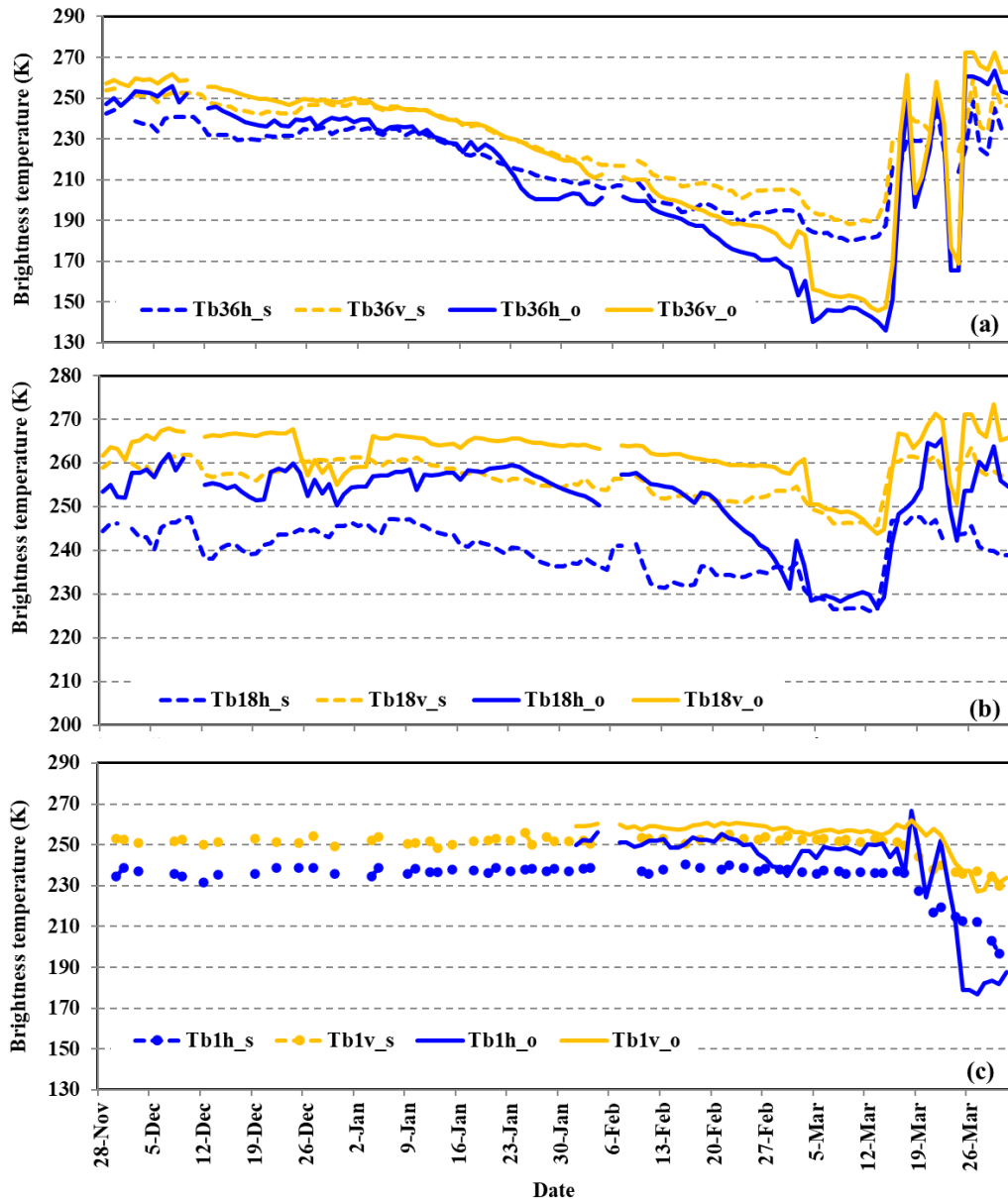
Figure 14. Comparison of brightness temperature between ground-based (o) and satellite-based observations (s), (a) for 36 GHz, (b) for 18 GHz, and (c) for 1.4 GHz.

4.4 4-component Radiation

The land surface albedo is strongly related to the land cover. In this experiment, the downward short-wave radiation presented general increase after January, while the trend became distinctive after February (Figure 15). The upward short-wave radiation abruptly increased when the ground was covered by snow (after November 21), and sharply declined on the snow off day (March 25). From the first snowfall by the end of January, the ratios between upward and downward short-wave radiation were approximately 95%. The ratio decreased with snow age, and in the end of snow season, the ratios decreased to approximately 25% on snow off day.
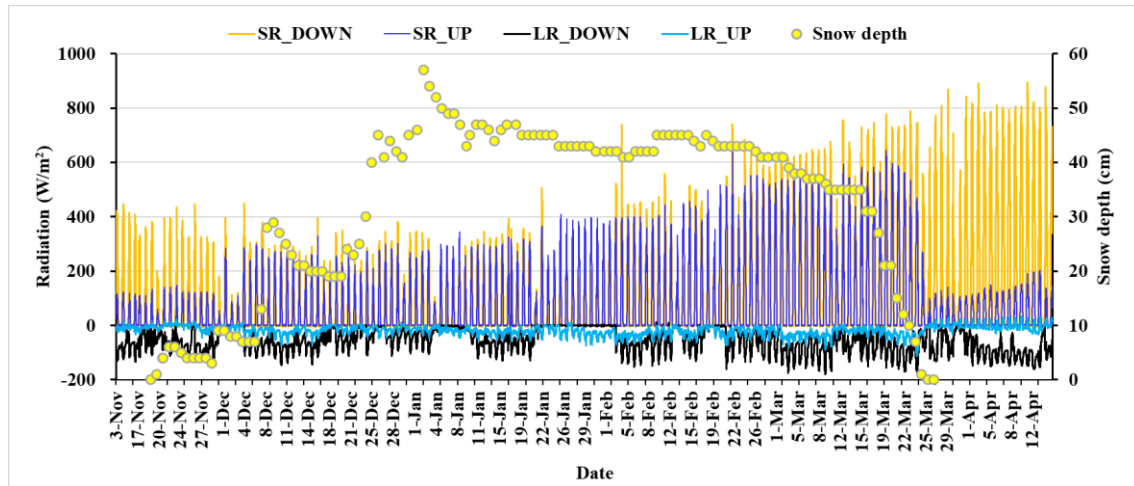
Figure 15. Minutely variation in 4-component radiation and daily variation in snow depth at Altay station from November 3, 2015 to April 15, 2016.

5 Discussion

5.1 Applications

Our dataset is, though for one snow season, provides daily snow pit observations with coincident microwave and optical radiation data, including comprehensive and detailed snow parameters, allowing researchers to find more details in snow characteristics and their relationship with remote sensing signatures. The dataset also fills the snow observation gap in mid-low snow depth area with relative short snow cover duration.

The snow pit data and microwave brightness temperatures have proven useful for evaluating and updating a microwave emission transfer model of snowpack (Dai et al., 2022). This dataset reflected a general fact that brightness temperature at higher frequencies presented stronger volume scattering of snow grains, and were more sensitive to snow characteristics. This experiment revealed that the dominant control for the variation of brightness temperature was the variation of grain size but not snow depth or SWE. In the stable period, brightness temperature difference between 18.7 and 36.5 GHz increased with growing grain size in the condition of dry snowpack. Therefore, the daily snow depth variations curve derived from passive microwave remote sensing datasets tend to exhibit a temporal offset from those of in situ observation.

During the snow season, brightness temperatures for both polarizations presented similar variation trends, though behaving different in fluctuation. The horizontal polarization was more sensitive to environment and was less stable than vertical polarization. Besides, the polarization difference at 18.7 GHz and 36.5 GHz showed increase and decrease trends, respectively, during the experimental period. This phenomenon was different from the simulation results (Dai et al., 2022). The different polarization behavior at 18.7 and 36.5 GHz might be related to the environmental conditions, snow characteristics and soil conditions. However, as the subsurface soil moisture was not observed, the dynamic ground emissivity could not be estimated. As it is known, as L band has strong penetrability, the brightness temperature variations were predominantly related to subsurface soil conditions, unless for the situations that the liquid water content within snowpack was high. Therefore, in the condition of soil moisture data absence, L band brightness temperatures were expected to reflect soil moisture variation that influences the soil transmissivity (Babaeian et al., 2019; Naderpour et al., 2017; Hirahara et al., 2020).

448   Snow surface albedo significantly influences the incoming solar radiation, playing an important role
449   in the climate system. The factors altering snow surface albedo contain the snow characteristics (grain
450   size, SWE, liquid water content, impurities, surface temperature etc), external atmospheric condition and
451   solar zenith angle (Aoki et al., 2003). Snow albedo was estimated based on snow surface temperatures
452   in some models (Roesch et al., 1999), while others considered that snow surface albedo was mainly
453   related to snow age (Mabuchi et al., 1997). In this experiment, we obtained the 4-component radiation,
454   snow pit and meteorological data, providing nearly all observations of possible influence factors,
455   therefore could be utilized to analyze shortwave radiation process of snowpack, and validate or improve
456   multiple-snow-layer albedo models.

457   Snow grain sizes and snow densities within different layers presented different growth rates during
458   different periods. Generally, the growth rates are related to the air temperature, pressure and snow depth
459   (Chen et al., 2020; Essery, 2015; Vionnet et al., 2012; Lehning et al., 2002); therefore, this dataset can
460   be used to analyze the evolution process of snow characteristics, as well as validation data for snow
461   models.

462   5.2 Uncertainties

463   During the experiment, some uncertainties were produced due to irresistible factors. It was reported
464   that the sampling depth of the L-band microwave emission under frozen and thawed soil conditions is
465   determined at 2.5 cm (Zheng et al., 2019). We did not collect subsurface soil moisture, and the L band
466   radiometer observation began on January 30, 2016. Therefore, it is difficult to obtain the ground
467   emissivity in the full snow season based on the data. The soil moisture data at 10 and 20 cm under
468   soil/snow interface cannot be directly used to validate and develop soil moisture retrieval from L band
469   brightness temperature. In the future, detailed soil moisture profile will be observed to estimate the
470   subsurface soil moisture to fill the gap.

471   The grain size data were collected through taking photos. When measuring the length of grains, the
472   grain selection has subjectivity, and the released data are statistic results based on the recorded grain
473   sizes. Although the general variation trend can be reflected by the time series of average grain size, some
474   details might be missed. Therefore, for who with interests, the original grain photos could be provided
475   through requesting for authors. In snowmelt period, large liquid water content would influence the
476   measurement results of snow fork. Therefore, it is suggested to use small-size snow shovel or cutter to
477   observe layered snow density in future experiments.

478   One season observation is quite valuable for developing and validate remote sensing snow retrieval
479   method or snow model, although the representativeness of this observation requires further analysis.
480   Nevertheless, more years of observations should be considered to increase the statistical significance of
481   the evolution of snow characteristics.

482   **6 Conclusions**

483   In a summary, the IMCS campaign provides snow pits observation, meteorological parameters,
484   optical radiation and passive microwave brightness temperatures in the snow season of 2015/2016. The
485   dataset is unique in providing microwave brightness temperatures and coincident daily snow pits data
486   over a full snow season at a fix site. The first use of our dataset is for the validation of snow microwave
487   emission models, improving its simulation accuracy.

488   The daily snow pit data provide snow grain size, grain shape, snow density and snow temperature
489   profiles. Generally, grain size grew with snow age, and increased from top to bottom. Snow grains are

rounded shape with small grain size in the top layer, and depth hoar with large grain size in the bottom layer. Snow density experienced increase-stable-increase variation, and the densities of the middle layers were greater than the bottom layer due to the well-developed depth hoar in the stable period. The data can be used to analyze the evolution process of snow characteristics combining with weather data, also for the validation and improvement of the snow process models, such as SNOWPACK (Lehning et al., 2002), SNTHERM (Chen et al., 2020), etc. The improvement of these snow process models can further enhance the prediction accuracy of land surface process and hydrology models.

Microwave radiometer data and snow pit data have been utilized to analyze the volume scattering features of snowpack at different frequencies (Dai et al., 2022). Results showed that grain size was the most important factor to influence snow volume scattering. The data can also be used for analysis of polarization characteristics of snowpack, combining with soil and weather data.

The microwave and optical radiations were simultaneously observed. Existing studies reported that the optical equivalent diameter must be used in microwave emission model with caution (Löwe and Picard, 2015; Roy et al., 2013). These data provide a new opportunity to analyze the difference between the influence of grain size on microwave and optical radiation, establishing the bridge between effective optical grain size and microwave grain size.

7 Data availability

The IMCS consolidated datasets are available on the National Tibetan Plateau Data Center and available online at http://data.tpdc.ac.cn/zh-hans/data/df1b5edb-daf7-421f-b326-cdb278547eb5/ (doi: 10.11888/Snow.tpdc.270886). Microwave radiometry raw Data are available for scientific use on request from Northwest Institute of Eco-Environment and Resources, Chinese Academy of Sciences.

Appendix

Figure A1. Photos of grains and reference ruler in each layer on February 15, 2016. In each photo the

longest and shortest axis lengths of the chosen grains are labeled. Original photos are in URL:

http://arcticroute.tpdc.ac.cn/navigate/bmp

Table A1. Recorded longest and shortest axis length in Figure A.

Stratigraphy	Thickness (cm)	Shape	Grain size (longest axis * shortest axis)(mm)								
the fifth	3cm	#22	0.595*0.436	0.472*0.471	0.450*0.436	0.615*0.474	0.374*0.314	0.647*0.307	0.656*0.529	0.544*0.519	0.717*0.447
			0.750*0.445	1.056*0.955	0.623*0.378	0.451*0.405	1.397*0.635	1.235*0.327	0.600*0.421	0.633*0.556	0.729*0.423
the fourth	3cm	#37	2.605*2.011	1.850*1.328	1.626*1.554	1.767*1.685	1.718*1.535	2.255*1.296	1.674*1.601	1.542*1.269	3.505*1.440
			3.055*1.774	1.448*1.37	2.461*1.914	2.757*2.115	2.179*2.059	2.393*1.788			
the third	25cm	#27, #31, #37	2.569*1.607	2.073*2.130	2.591*1.414	1.869*1.802	2.067*1.266	1.209*1.106	1.719*1.188	1.648*0.975	1.911*1.582
			1.921*1.710	1.518*1.067	1.291*1.147	1.690*1.551	1.756*1.398	1.812*1.263	1.733*1.672	1.880*1.518	2.411*1.220
			2.118*1.727	1.614*1.457	1.795*1.705	2.215*2.311	1.864*1.692	1.967*1.651	2.008*1.395	1.362*1.141	1.484*1.291
the second	12	#33, #34	4.251*2.266	3.012*2.65	2.805*1.995	1.799*1.415	1.402*1.195	3.040*2.073	2.850*2.095		
			3.900*2.532	2.420*2.333	2.515*2.206	2.044*2.032	2.506*2.363	2.894*2.161	2.413*1.950	2.494*1.816	4.929*3.257
the first	4	#40, #34, #38	4.933*3.378	3.207*2.774	3.562*1.701	2.818*1.668	3.581*2.518	6.179*3.562			

547 **Table A2. An example of record table for snow density observation.**

Observation date: 20160111; Observation time: 9:03-9:40; Weather: clear; Snow depth: 48cm						
Snow tube table						
Snow depth(cm)		46.5		47		47.5
Snow pressure(g/cm^2)		9.1		9		9.5
Snow density(g/cm^3)		0.1957		0.1915		0.2000
Snow Folk table			**Snow shovel table**			
Observation height（cm）	Liquid water content (%)	Snow density（g/cm^3）	Observation layer (cm)	Weight of shovel+snow (g)	Weight of shovel (g)	Snow density (g/cm^3)
5	0	0.1923	0-10	865.04	572.16	0.1953
	0.118	0.1882		858.72	572.16	0.1910
	0	0.1882		866.69	572.16	0.1964
10	0.461	0.164				
	0.46	0.1631				
	0.461	0.1361				
15	0.123	0.2532	10-20	878.58	572.16	0.2043
	0	0.2506		887.04	572.16	0.2099
	0	0.2417		872.79	572.16	0.2004
20	0.24	0.2159				
	0.119	0.2155				
	0.119	0.2146				
25	0.117	0.1977	20-30	905.34	572.16	0.2221
	0	0.1994		903.41	572.16	0.2208
	0	0.1984		907.88	572.16	0.2238
30	0	0.1919				
	0	0.1966				
	0	0.1928				
35	0	0.1534	30-40	832.75	572.16	0.1737
	0	0.1517		838.14	572.16	0.1773
	0	0.1472		837.27	572.16	0.1767
40	0.325	0.1097				
	0	0.1054				
	0.107	0.1088				
45	0	0.0922				
	0	0.0991				
	0	0.0928				

548
549

References:

Aoki, T., Hachikubo, A., and Hori, M.: Effects of snow physical parameters on shortwave broadband albedos, J. Geophys. Res-Atmos., 108 (D19), 4616, https://doi.org/10.1029/2003JD003506, 2003.

Babaeian, E., Sadeghi, M., Jones, S.B., Montzka, C., Vereecken, H., and Tuller, M.: Ground, Proximal, and Satellite Remote Sensing of Soil Moisture, Rev. Geophys., 57(2), 530-616, https://doi.org/ 10.1029/2018RG000618, 2019.

Brucker, L., Hiemstra, C., Marshall, H.-P., Elder, K., De Roo, R., Mousavi, M., Bliven, F., Peterson, W., Deems, J., Gadomski, P., Gelvin, A., Spaete, L., Barnhart, T., Brandt, T., Burkhart, J., Crawford, C., Datta, T., Erikstrod, H., Glenn, N., Hale, K., Holben, B., Houser, P., Jennings, K., Kelly, R., Kraft, J., Langlois, A., McGrath, D., Merriman, C., Molotch, N., Nolin, A., Polashenski, C., Raleigh, M., Rittger, K., Rodriguez, C., Roy, A., Skiles, M., Small, E., Tedesco, M., Tennant, C., Thompson, A., Tian, L., Uhlmann, Z., Webb, R., and Wingo, M.: A first overview of snowex ground-based remote sensing activities during the winter 2016-2017, Int. Geosci. Remote Sen., 1391-1394, http://dx.doi.org/10.1109/IGARSS.2017.8127223, 2017.

Chen, T., Pan, J.M., Chang, S.L., Xiong, C., Shi, J.C., Liu, M.Y., Che, T., Wang, L.F., and Liu, H.R.: Validation of the SNTHERM Model Applied for snow depth, grain size, and brightness temperature simulation at meteorological stations in China, Remote Sens., 12, 507, https://doi.org/Artn 50710.3390/Rs12030507, 2020.

Cline, D., Elder, K., Davis, B., Hardy, J., Liston, G., Imel, D., Yueh, S., Gasiewski, A., Koh, G., Amstrong, R., and Parsons, M.: An overview of the NASA Cold Land Processes Field Experiment (CLPX-2002), P. Soc. Photo-Opt. Ins., 4894, 361-372, https://doi.org/ 10.1117/12.467766, 2003.

Dai, L.: Microwave radiometry experiment data in Altay (2015/2016), National Tibetan Plateau Data Center [dataset], https://doi.org/10.11888/Snow.tpdc.270886, 2020.

Dai, L.Y., Che, T., Xiao, L., Akynbekkyzy, M., Zhao, K., and Leppänen, L.: Improving the Snow Volume Scattering Algorithm in a Microwave Forward Model by Using Ground-Based Remote Sensing Snow Observations, Ieee T. Geosci. Remote., 60, 4300617, https://doi.org/10.1109/TGRS.2021.3064309, 2022.

Derksen, C., Toose, P., Lemmetyinen, J., Pulliainen, J., Langlois, A., Rutter, N., and Fuller, M.C.: Evaluation of passive microwave brightness temperature simulations and snow water equivalent retrievals through a winter season, Remote Sens. Environ., 117, 236-248, https://doi.org/ 10.1016/j.rse.2011.09.021, 2012.

Essery, R.: A factorial snowpack model (FSM 1.0), Geosci. Model Dev. 8, 3867–3876, https://doi.org/10.5194/gmd-8-3867-2015, 2015.

Fierz, C., Armstrong, R.L., Durand, Y., Etchevers, P., Greene, E., McClung, D.M., Nishimura, K., Satyawali, P.K. and Sokratov, S.A.: The International Classification for Seasonal Snow on the Ground. IHP-VII Technical Documents in Hydrology N°83, IACS Contribution N°1, UNESCO-IHP, Paris, 2009.

Hirahara, Y., de Rosnay, P., and Arduini, G.: Evaluation of a microwave emissivity module for snow covered area with CMEM in the ECMWF Integrated Forecasting System, Remote Sens., 12(18), https://doi.org/ 10.3390/rs12182946, 2020.

Lehning, M., Bartelt, P., Brown, B., Fierz, C., and Satyawali, P.: A physical SNOWPACK model for the Swiss avalanche warning Part II: Snow microstructure, Cold Reg. Sci. Technol., 35, 147-167, https://doi.org/ 10.1016/S0165-232x(02)00073-3, 2002.

Lemmetyinen, J., Kontu, A., Pulliainen, J., Vehvilainen, J., Rautiainen, K., Wiesmann, A., Matzler, C., Werner, C., Rott, H., Nagler, T., Schneebeli, M., Proksch, M., Schuttemeyer, D., Kern, M., and Davidson, M.W.J.: Nordic Snow Radar Experiment, Geosci. Instrum. Meth., 5, 403-415, https://doi.org/10.5194/gi-5-403-2016, 2016.

Li, X., Che, T., Li, X. W., Wang, L., Duan, A. M., Shangguan, D. H., Pan, X. D., Fang, M. and Bao, Q.: CASEarth Poles Big Data for the Three Poles, B. Am. Meteorol. Soc., 101(9): E1475-E1491, https://doi.org/10.1175/Bams-D-19-0280.1, 2020.

Löwe, H. and Picard, G.: Microwave scattering coefficient of snow in MEMLS and DMRT-ML revisited: The relevance of sticky hard spheres and tomography-based estimates of stickiness, Cryosphere, 9(6), 2101–2117, https://doi.org/10.5194/tc-9-2101-2015, 2015.

Mabuchi, K., Sato, Y., Kida, H., Saigusa, N. and Oikawa, T.: A biosphere-atmosphere interaction model (BAIM) and its primary verification using grassland data, Pap. Meteorol. Geophys., 47, 115–140, https://doi.org/10.2467/mripapers.47.115, 1997.

Naderpour, R., Schwank, M., Matzler, C., Lemmetyinen, J., and Steffen, K.: Snow Density and Ground Permittivity Retrieved From L-Band Radiometry: A Retrieval Sensitivity Analysis. Ieee J-Stars., 10(7), 3148-3161, https://doi.org/10.1109/Jstars.2017.2669336, 2017.

Pan, X. D., Guo, X. J., Li, X., Niu, X. L., Yang, X. J., Feng, M., Che, T., Jin, R., Ran, Y. H., Guo, J. W., Hu, X. L. and Wu, A. D.: National Tibetan Plateau Data Center Promoting Earth System Science on the Third Pole, B. Am. Meteorol. Soc., 102(11), E2062-E78, https://doi.org/Bams-D-21-0004.1, 2021.

Roesch, A., Gilgen, H., Wild, M., and Ohmura, A.: Assessment of GCM simulated snow albedo using direct observations, Clim. Dynam., 15, 405– 418, https://doi.org/10.1007/s003820050290, 1999.

Roy, A., Picard, G., Royer, A., Montpetit, B., Dupont, F., Langlois, A., Derksen, C., and Champollion, N.: Brightness Temperature Simulations of the Canadian seasonal snowpack driven by measurements of the snow specific surface area, Ieee T. Geosci. Remote., 51, 4692-4704, https://doi.org/10.1109/Tgrs.2012.2235842, 2013.

Royer, A., Roy, A., Montpetit, B., Saint-Jean-Rondeau, O., Picard, G., Brucker, L., and Langlois, A.: Comparison of commonly-used microwave radiative transfer models for snow remote sensing, Remote Sens. Environ., 190, 247-259, https://doi.org/10.1016/j.rse.2016.12.020, 2017.

Tedesco, M., and Kim, E.J.: Intercomparison of electromagnetic models for passive microwave remote sensing of snow, Ieee T. Geosci. Remote., 44, 2654-2666, https://doi.org/ 10.1109/TGRS.2006.873182, 2006.

Vionnet, V., Brun, E., Morin, S., Boone, A., Faroux, S., Le Moigne, P., Martin, E., and Willemet, J.M.: The detailed snowpack scheme Crocus and its implementation in SURFEX v7.2, Geosci. Model Dev., 5, 773-791, https://doi.org/10.5194/gmd-5-773-2012, 2012.

Zheng, D., Li, X., Zhao, T., Wen, J., van der Velde, R., Schwank, M., Wang, X., Wang, Z., and Su, Z.: Impact of soil permittivity and temperature profile on L-Band microwave emission of frozen soil. Ieee T. Geosci. Remote., 59(5), 4080-4093, https://doi.org/10.1109/TGRS.2020.3024971, 2021.

Zhang, P., Zheng, D., van der Velde, R., Wen, J., Zeng, Y., Wang, X., Wang, Z., Chen, J., and Su, Z.: Status of the Tibetan Plateau observatory (Tibet-Obs) and a 10-year (2009–2019) surface soil moisture dataset, Earth Syst. Sci. Data, 13, 3075–3102, https://doi.org/10.5194/essd-13-3075-2021, 2021.

Zheng, D., Li, X., Wang, X., Wang, Z., Wen, J., van der Velde, R., Schwank, M., and Su, Z.: Sampling depth of L-band radiometer measurements of soil moisture and freeze-thaw dynamics on the Tibetan Plateau, Remote Sens. Environ., 226, 16-25, https://doi.org/10.1016/j.rse.2019.03.029, 2019.